Ultrasound Flow-Monitoring and Flow-Metering of Air–Oil–Water Three-Layer Pipe Flows

JUNPEI HITOMI, YUICHI MURAI, HYUN JIN PARK, AND YUJI TASAKA
Laboratory for Flow Control, Division of Energy and Environmental Systems, Faculty of Engineering, Hokkaido University, Sapporo 060-8628, Japan
Corresponding author: Yuichi Murai (murai@eng.hokudai.ac.jp)

ABSTRACT The combined use of ultrasound pulse-echo intensity and Doppler shift frequency is examined as a means to measure strong unsteady three-phase pipe flows of a gas and two liquids. With air, oil, and water as components of the fluid media, particular attention is given to analyze ultrasound responses at the air–oil and oil–water interfaces. Reciprocating slugging is generated inside a 55-mm-diameter circular pipe, of which edges oscillate vertically at a controlled frequency. We use an ultrasound velocity profiler to obtain the 1-D cross-sectional distributions of the instantaneous flow velocity at the sampling rate of 60 Hz. All the measurements are realized by a single ultrasound transducer located outside the pipe. Measurement accuracy is validated using a high-speed camera coupled with particle image velocimetry that is synchronized with the profiler. The results demonstrate that the proposed technique works properly in sensing both interfaces as well as in-phase flow velocity distributions. In addition, multiphase volume flow rates for the constituents are obtained by velocity profile integration assuming vertical phase stratification in an approximation.

INDEX TERMS Doppler method, flow metering, multiphase flow, particle image velocimetry, pipe flow, pipe line, ultrasound

I. INTRODUCTION

Using ultrasound Doppler information for flow metering is a non-invasive, first-principle-based measurement [1]. The volume flow rate is directly given by area integration of the spatial distribution of the velocity within a target plane. Distinct from ordinary indirect flow-metering devices, no calibration is required preliminarily because of the capability of velocity distributions [2]. This feature enables the target of flow metering to be expanded widely such as for curved flows [3], non-Newtonian flows [4]–[6], and for multiphase flows [7]–[19]. In particular, the application to multiphase flow is challenging. Conventional approaches to flow metering of multiphase flows are such that an individual phase needs to be sufficiently separated for the metering device to be effective. Alternatively, homogeneous mixing allows the devices to approximate the flow rate [20]. However, such phase-control operations require a change in pipeline systems and invariably experiences a significant pressure loss. Therefore, for large systems such as in power and chemical plants, a non-invasive approach along with related technology to monitor directly internal multiphase flows is keenly waited to be developed.

To handle the strong unsteady three dimensionality of multiphase pipe flows in the measurement section, several strategies are now being developed such as by electric capacitance [21], [22], by optical rays [23], [24], and acoustic approaches. Among various non-invasive monitoring principles, ultrasound has multiple advantages in comparison with others. One is access to opaque fluids such as chemical solutions, fuel oils, and their suspensions. Another is spatial resolution, which suffices to monitor internal flow structures with a control of basic wavelength of ultrasound. As the sensors can be located outside the pipe, portability and easy-to-mount operation are further additional benefits to consider wide industrial applications. The known disadvantage, conversely, is the damping of weak ultrasound pulses during propagation in fluid media. Users should also take care of acoustic noise from multiple reflections of pulses in the acoustic environment around the measurement section.

In our previous series of developments, we found how to extract position of the fluid–fluid interface from the ultrasound pulse waveform in echoes from multiphase flows. For gas–liquid combinations, three kinds of waveform analysis were proposed to obtain automated interfacial detection [15]. Based on the technique, we also developed an ultrasound void-fraction profiler [11] and ultrasound viscometry [17] for bubbly two-phase flow regimes. In the present work, we apply such ultrasonic sensing to three-phase pipe flows of gas–liquid–liquid stratifications. The demand for three-phase flow measurements have risen in the fuel pipe line industry

where oil and water co-flow with a gas component. Such flows have a contrasting variety of flow patterns depending on the combination of three flow rates. The local flow structure must be monitored for stable continuous fuel transport as well as security from the risk of pulsatile behavior. Similar issues exist in chemical plants that handle complex multiphase flows consisting of phases of largely different properties.

To meet these demands, we investigated specifically air–oil–water pipe flows to assess whether the ultrasound pulse technique is applicable. For the platform of experimentation, a seesaw type of oscillating three-phase pipe flow system was built (Fig. 1). Using this system, we obtained multiple interface echoes from a single sequence of ultrasound pulse emissions, and in-phase velocity profiling. From echo intensities and Doppler frequencies, we were able to examine flow metering to estimate the volume flow rates of each phase. The accuracy of the method is validated by particle image velocimetry enabling measurement error to be evaluated and the dynamics of three-phase pipe flows to be quantified.
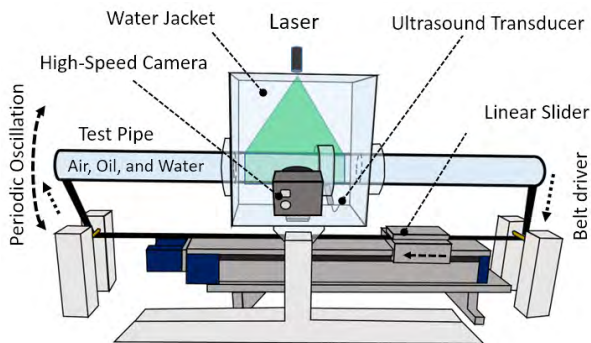

FIGURE 1. Seesaw-driven multiphase pipe flow facility. Three phases are filled in the pipe with end plates on both edges, and oscillated by a single belt connected with a computer controlled linear slider. UVP and high-speed video imaging are conducted on the oscillation frame.

II. EXPERIMENTATION PLATFORM

For the seesaw-driven facility (Fig. 1), the pipe diameter and length are $D = 55$ mm, and $L = 1000$ mm, respectively. To record the flow optically the pipe was made of transparent acrylic resin.

Both ends of the pipe are connected to a single moving belt driven by a motor linear slider. The motion of this slider is controlled by a PC, which regulates the amplitude and frequency of the pipe ends. The maximum amplitude and frequency are 200 mm and 1.0 Hz. Air, oil, and water enter the pipe at the laboratory temperature of 25 °C. The test oil was Silicone oil of kinematic viscosity 10 cSt and density of 935 kg/m^3 and is immiscible with water.

A. ULTRASOUND INSTRUMENTATION

Three kinds of measurement instrumentation were introduced to the platform providing ultrasound monitoring, backlight visualization, and laser sheet illumination.

For ultrasound monitoring, an ultrasound transducer is set beneath the pipe at 15° to the pipe cross sectional plane.

The transducer is submerged in a water jacket so that the propagation of the pulse into the pipe interior is easier as well as its return echo to the transducer. The water jacket is a cubic buffer tank with side length of 255 mm, sufficient to eliminate ultrasound residuals from around as the measurement section is monitored at 2 kHz in pulse repetition frequency. The transducer emits and receives periodic ultrasound pulse of 4 MHz in basic frequency. The nominal intensity of the emitted pulse is 150 V whereas the echo intensity level is only of an order of a few millivolts. The effective diameter of the ultrasound pulse is 5 mm. The cycle number of the pulse is set to 4. Therefore, the spatial resolution in water is estimated to be a 5 mm-diameter disk of thickness $4[(1497 \text{ m/s})/(4 \times 10^6 \text{ Hz})]/2 = 0.75$ mm, where 1497 m/s is the speed of sound in the experiment. The temporal resolution is given by the sampling rate of Doppler velocity profiling in the ultrasound velocity profiling (UVP) operation, which is 60 Hz under present conditions.

B. OPTICAL FLOW VISUALIZATION

To verify the ultrasound monitoring performance, two kinds of optical flow visualization were applied. One is backlight projection of the phase distribution [Fig. 2(a)], in which oil is dyed red, the dye being solvable in oil but insolvable in water. For water, aqueous green food dye was mixed in to identify the oil–water interface as contrast between red and green colors. Diffused white light of 650-W power illuminated the pipe from behind to enable a backlight color projection video image to be recorded. The camera was set up on the opposite side of the light source.
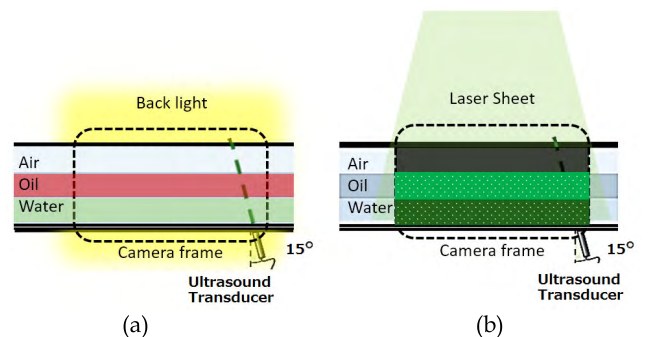

FIGURE 2. Methods for visualizing the flow: (a) white backlighting of dyed liquids to see the projection phase distributions, and (b) laser sheet illumination of central plane where UVP measurement line is applied.

The other is laser illumination of the oil and water phases for PIV measurements. For water, high-porous polymer particles were used as the tracers. The particles have a density of 1010 kg/m^3 and were 80 to 120 μm in diameter. For oil the tracers were water-repellent solid particles of density 920 kg/m^3 and peak diameter 110 μm. We observed that a small percentage of the particles adhered to the air–oil and the oil–water interfaces. Whereas the adhesion may change the interfacial property slightly, the Weber number (to be explained later) was kept high enough to have an

insignificant effect on the dynamic behavior of the three-phase flow. Moreover, the laser sheet scatters on the interfaces because of the adhesion, which assisted in viewing the two interfaces. The number density of tracer particles in each phase is guaranteed due to periodic wave-breaking generated on both interfaces during the oscillatory motion of the pipe.

Fig. 3 shows how each phase behaves during a single 5-s-period cycle of the seesaw motion of the pipe. Left and right rows correspond with rightward and leftward flows driven by the pipe inclination. Note that the camera is mounted on the same oscillation frame so that consecutive images depict interfacial motions relative to the pipe wall. The pipe-bulk volume fractions of air, oil, and water are set to 1/3. The oil layer produces a wave-breaking front that rapidly propagates in the air–oil interface at $t = 1.0$ s and $t = 3.5$ s. Water accelerates slowly with a time lag of $t = 1.5$ s and $t = 4.0$ s after wave propagation in the upper oil phase. During this cycle, capillary waves move along the oil–water interface due to shear stress transfer through the interface. Slightly dark spots observed along both interfaces indicate wavy surfaces that accompany three-dimensional interfacial structures. Apart from these spots, the main flow is confirmed to be approximately two-dimensional.
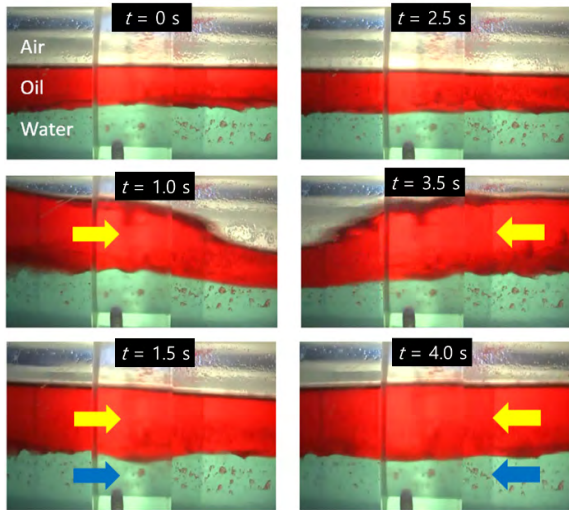

FIGURE 3. Cyclic behavior of the three-phase flow visualized using color projection in a single cycle of the pipe oscillation.

Fig. 4 presents the time-line image of the phase distribution, sampled from the video image. The sampling line is set vertically at the same position of the UVP measurement (to be described below). As the time-line image shows, the air–oil interface repeats a sharp rise and slow fall in every cycle whereas the oil–water interface fluctuates at a higher frequency but with small amplitude. With diverse combinations of volume ratios of air, oil, and water, many different types of interfacial behavior were observed. From these characteristics of the interfacial motion, ultrasound monitoring is examined.
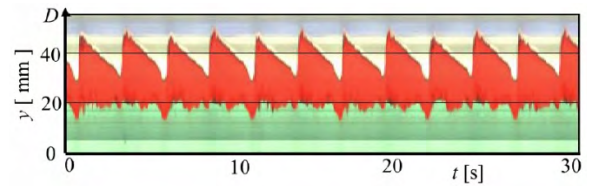

FIGURE 4. Time-line image of the three-phase flow at the central plane of the oscillating pipe, showing wavy passage of oil and water phases with different interfacial structures observed at the oscillation period of $T = 5$ s.

Fig. 5 presents the same time sequence of tracer particle images illuminated by a laser sheet. These images are processed by PIV software to verify the results from ultrasound measurements.
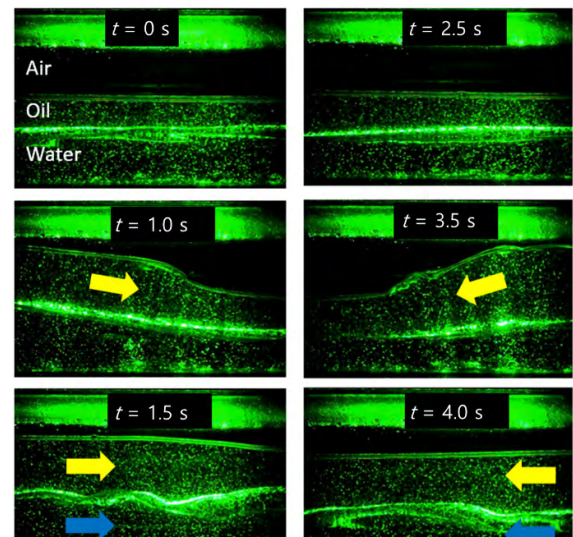

FIGURE 5. Particle images for PIV measurements, in which fluid interfaces at the central plane are also visualized.

III. RESULTS AND DISCUSSION

To analyze the data, for the oscillating three-phase pipe flow, dimensionless parameters are introduced:

$$Re_j = \frac{\rho_j D U}{\mu_j}, \quad j = \{a, o, w\}, \tag{1}$$

$$Fr_{jk} = \frac{U}{\sqrt{gD\left(\Delta\rho_{jk}/\rho_j\right)}}, \quad jk = \{a/o, o/w\} \tag{2}$$

$$We_{jk} = \frac{\rho_j U D}{\sigma_{jk}}, \tag{3}$$

where D and U denote the pipe diameter and bulk mean flow velocity, respectively. Subscripts a, o, and w denote the phase of air, oil, and water, respectively. The range of D treatable by the present ultrasound sensing is from 20 to 100 mm while we fix $D = 55$ mm in the present demonstration. There are hence three Reynolds numbers—two Froude numbers, and two Weber numbers—giving a total of seven dimensionless parameters. In each definition, the characteristic speed of

the flow U is given by the pipe oscillation frequency F and amplitude H,

$$U = 2\pi F H \qquad (4)$$

In the present range of test measurements, Re has order $O(10^5)$ in water, $O(10^4)$ in air, and $O(10^3)$ in oil. This implies that the air–water interface is influenced by in-phase turbulence whereas the oil phase belongs to a transitional regime. Fr has order $O(1)$ for air–water and $O(10)$ for oil–water interfaces, evidencing the emergence of a wave-breaking front on both interfaces. The two Weber numbers are of order $O(10)$ corresponding to a characteristic length scale of a few millimeters for capillary waves that may appear on the interfaces.

Hence, the ultrasound sensing performance is assessed for all the above-mentioned flow elements stemming from within the three-phase flow, such as turbulence in each phase, density stratification, gravity-induced waves, shear-induced capillary waves, and periodic flow sandwiched by the two neighbor interfaces.

A. ECHO INTENSITY AND DOPPLER VELOCITY

Prior to the experiment, we estimated the transmittance and reflectance of ultrasonic waves in the three-phase pipe flow including the pipe wall. Fig. 6 shows the result of the estimation with the three phases stratified vertically. With the ultrasound transducer set at the bottom of the pipe directed upward, echoes are received from six interfaces that exist between the transducer and the counter surface of the pipe. At each interface, formed between two media with acoustic impedances Z_1, and Z_2, the reflection ratio of ultrasound is

$$R = \frac{Z_2 - Z_1}{Z_2 + Z_1}, \qquad \begin{cases} Z_1 = \rho_1 C_1 \\ Z_1 = \rho_1 C_1 \end{cases} \qquad (5)$$

where ρ and C are density and speed of sound, respectively. The acoustic pressure $A.P.$ of the ultrasound wave that propagates directly beyond multiple interfaces is

$$A.P. = (1 - R_1)(1 - R_2)\cdots = \prod_{k=1}^{K}(1 - R_k). \qquad (6)$$

Here the acoustic pressure is normalized by the value of the initial pressure of the emitted wave. In the present configuration, the values of the refection ratios R and the acoustic pressure $A.P.$ are obtained (Fig. 6). The acoustic pressure decreases to 0.30 in water, decreases further to 0.26 in oil, and almost disappears below 10^{-5} in air. The acoustic pressure of echoes that the transducer receives is further weakened by the square impact from $A.P.$ because of shuttled propagation. Therefore we ignore the echo signal from the air phase as its acoustic pressure is below the sensing limit $O(10^{-5})$. Moreover, the echo from the air–oil and the oil–water interfaces are expected to be sufficiently strong as their pressure estimates are 0.07 and 0.01, respectively.
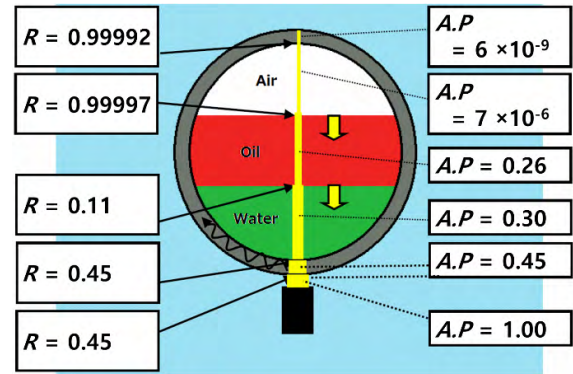

FIGURE 6. Schematic of ultrasonic transmission via six interfaces along the straight path subject to different reflection ratio *R* and penetration of acoustic pressure *AP*.
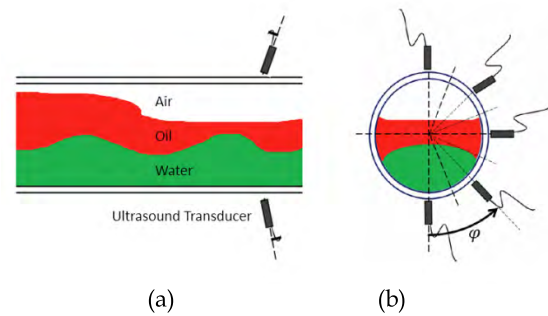

(a) (b)

FIGURE 7. Position of ultrasound transducer for examination of orientation dependent signal characteristics. (a) Side view. (b) Cross-section view.

With the estimation, we examined the signal quality of the echo by changing the angle of inclination of the transducer (Fig. 7). The results obtained (Fig. 8) were for equal volume ratios of three phases in the pipe, which oscillated at $F = 0.2$ Hz. The left and right columns present the echo intensity and Doppler velocity, respectively. Echo intensities were originally recorded as electric voltages with both positive and negative signs of an order of millivolts, and subsequently normalized in a linear scale by the lowest limit of sensible voltage. Doppler velocities were computed from the Doppler frequency shift involved in echo waveforms, the basic frequency of ultrasound, and the speed of sound. With the transducer inclined at $\varphi < 60°$, the two interfaces are identifiable in the echo intensity plots. At $\varphi = 90$, the interfaces no longer appear because from the for geometry the horizontal ultrasound pulses miss them. At $\varphi > 120$, the echoes disappear completely because pulses encounter the first air phase blocking transmission to the liquid phases. From the Doppler velocity profiles, the fluid motion is properly captured with repeated cycles of oil and water phases. However, Doppler velocities do not include any obvious information on interfacial position, but rather give a virtual velocity for the air phase. Next a method is described that eliminates this velocity.
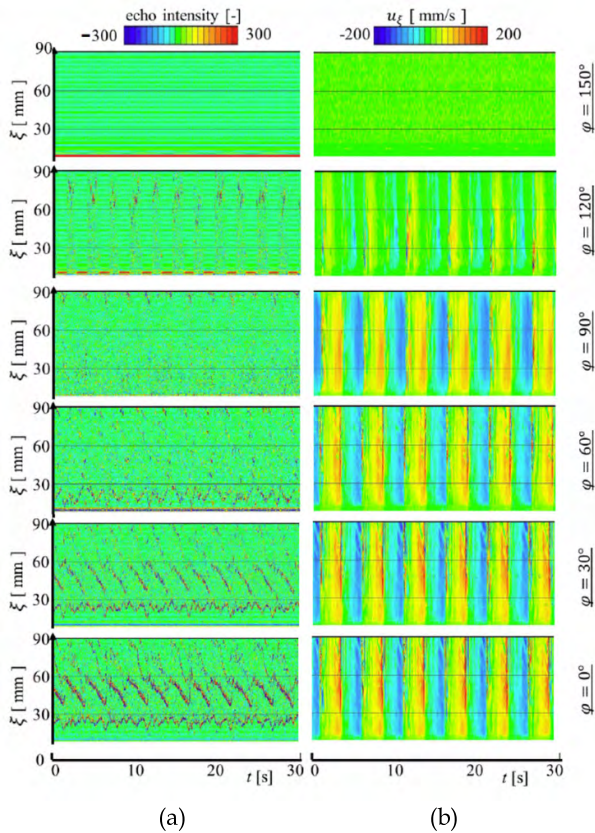
FIGURE 8. Difference in echo intensity and Doppler velocity involved in the pulse waveforms taken in six different angles. (a) Echo intensity. (b) Doppler velocity.

B. METHOD OF INTERFACE DETECTION

With a significant echo intensity confirmed from both interfaces, we analyze the echo data to detect these interfaces automatically.

The procedure (see outline in Fig. 9) involves first, applying a median filter to reduce pixel noise associated with the time-space echo distribution. The size of a single pixel is defined by the temporal sampling frequency and the spatial sampling interval. Next, echo amplitudes are computed from the enveloping function, taking positive values over the entire domain. In this step, two sharp peaks appear in the spatial coordinates (middle graph of the figure) corresponding to the positions of the air–oil and oil–water interfaces. A threshold is given to detect the central coordinates of the intensity peaks. The threshold value can be determined reductively from the above-mentioned theoretical reflections. However, the reflections in actual situations are complicated through the influence of turbulence, beam divergence, and, capillary waves. Therefore, we determine the threshold from a recursive approach, selecting its value at which two positions of the strong echo are always detected. This threshold value is automatically computable from a statistical analysis of the echo data, and is relatively robust to the various flow behaviors taking place.

The three-phase identification realized by the present interface detection is shown in Fig. 10. The figure involves
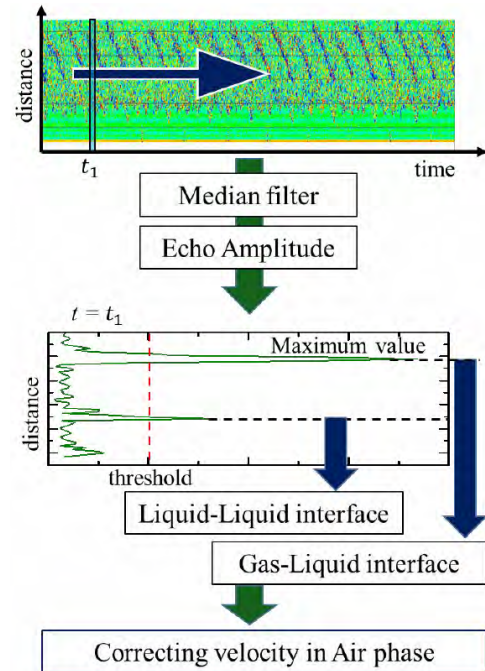

FIGURE 9. Flow chart of UVP-data processing with interface detection to classify the domain into gas, oil, and water phases.
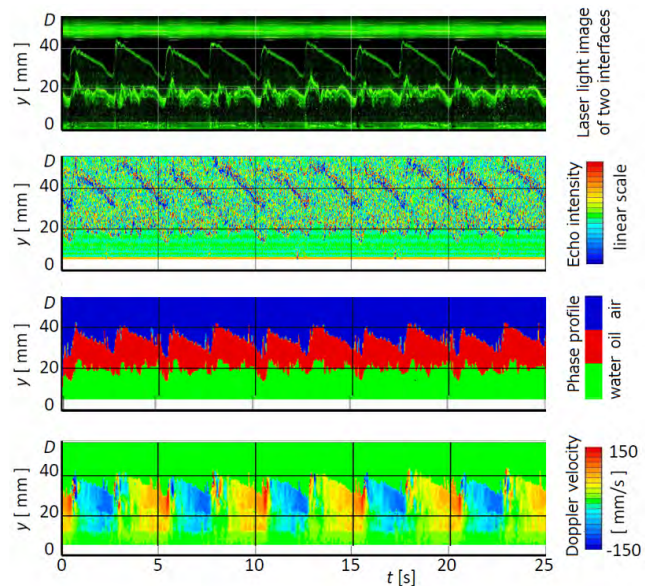

FIGURE 10. Samples of interface detection: (a) optical visualization, (b) echo intensity distribution, (c) phase distribution, and (d) Doppler velocity distribution.

individual time-line images of (a) the laser illumination of the two interfaces, (b) the echo intensity distribution, (c) the identification of the three-phase distribution, and (d) Doppler velocity profiles inside the oil and water phases. Regarding phase identification, some peaked errors remain at the air–oil interface in comparison with the color backlight visualization (see Fig. 4). These errors come from miss-detection of the air–oil interface due to sharp inclines in the local interface,

from where no echoes are received. Nevertheless, the three-phase flow structure is captured with acceptable accuracy for general purposes such as for measurements of volume fractions, constituent volume flow rates, and spectral analysis of interface displacements.

C. FLOW VELOCITY PROFILING COMPARED WITH PIV

The flow velocity distribution in the oil and water are obtained from Doppler velocities using the ultrasound velocity profiling technique (UVP). There are two main concerns when UVP is applied to two kinds of co-flowing liquids in a single measurement section. One is the pulse refraction at the oil–water interface when inclined non-perpendicularly to the propagating direction of the pulse. The other is multi-dimensional flow events excited in the three-phase flow, which UVP cannot detect because velocity profiling is one dimensional. To quantify these features, particle image velocimetry (PIV) of the flow field is employed.

From raw PIV data taken over a single cycle of the pipe oscillation, we extracted a time series of instantaneous flow velocity distributions. (Fig. 11); the magnitude of velocity vector is color coded. Here the pipe oscillation period is set at $T = 5.0$ s (hence the frequency is $F = 0.2$ Hz). The absence of local PIV data occurs in the result because the intensity of laser light saturates and incorrectly correlates the particle image in regions of rapid distortion in the fluid. After an adequate spatial interpolation is applied, a single vertical line along the same position of UVP is chosen to reproduce the time-line image of the velocity distribution (Fig. 12). Here the data for both UVP and PIV are the components of the flow velocity in the direction of ultrasound pulse propagation, i.e., 15° to the plane perpendicular to the axial direction of the pipe. From the figure, the UVP and PIV data exhibit strong similarities. Discrepancies in the data from the air–oil interface are attributable to absences of corresponding PIV data.

A more quantitative comparison (Fig. 13) is obtained from flow velocity fluctuations at mid-height in the oil phase ($y = 25$ mm from the bottom) and in the water phase ($y = 15$ mm). In the velocity computation from Doppler shift frequency, values for the speed of sound in oil and water are inputted, obtained already from information gleaned from the oil–water interface. In all tests under different flow conditions, the velocity magnitude of the oil phase from UVP is always larger than that from PIV. The ratio of the root-mean-square value of UVP to PIV ranges between 1.20 and 1.25. The high value is attributed to the mean dynamic inclination of the oil–water interface induced by slugging waves. In the water phase, such a bias is less than 10%. Note though that acoustic refraction on a flat oil–water interface, which has a refraction index of $n = 1.53$, does not directly induce such bias error in the resultant velocity in the oil phase. The reason is simply that the pulse propagates both ways. In water-to-oil transmission, the pulse bends with refractive index n. From its own echo, it transmits a returning pulse propagating from oil to water that bends depending on the reciprocal index n^{-1} that
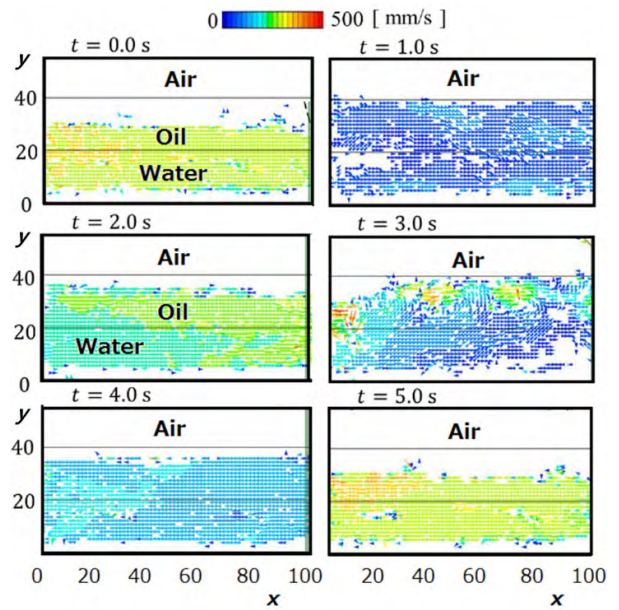

FIGURE 11. Instantaneous PIV data obtained inside the two liquid phases at six different timing within a single oscillation.
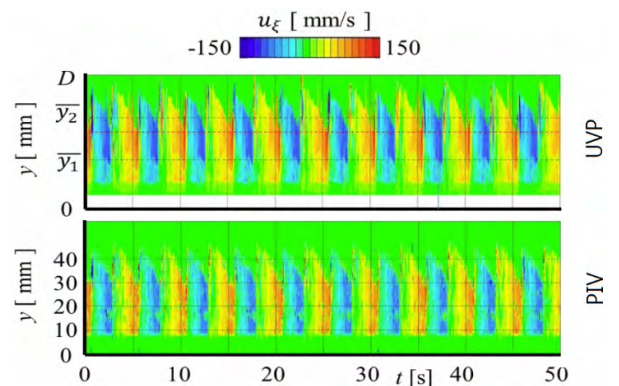

FIGURE 12. Comparison of fluid velocity data between UVP and PIV where PIV data are extracted on the same line of UVP.

cancels out refraction in the oil phase. The present bias of the velocity magnitude is therefore attributed to curvature effects of the interface arising from the dynamics of multiphase flow.

D. CONSTITUENT FLOW RATES

In addressing our final objective, constituent volume flow rates of the three-phase flow were estimated from the measured information. The present technique provides a one-dimensional three-phase flow measurement that, in principle, lacks information to correctly estimate the flow rates. An approximation model of the phase distribution is introduced for this estimation.

In testing this approach, we modeled the local phase distribution as a simple vertical stratification of the three layers (Fig. 14). In this model, a single transducer is placed at the bottom of the pipe. The flow rate of each phase is computed using the area integration of the velocity distribution within
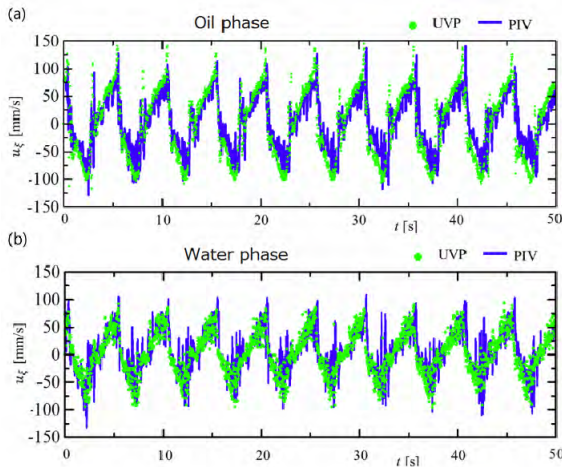
FIGURE 13. Flow velocity fluctuations in (a) the oil phase at *y* = 25 mm and (b) the water phase at *y* = 15 mm.

FIGURE 14. Velocity profile integration: (a) side view, (b) cross-section view, and (c) definition of $u_x(y)$.

FIGURE 15. Instantaneous volume flow rates measured by cross-sectional integration of axial velocity profile for each phase.

the border of the target phase,

$$Q(t) = \int_A u_x(y, z) dy dz, \tag{7}$$

where u_x is the flow velocity along the axial direction of the pipe, and *(y,z)* are the two-dimensional coordinates in its cross-sectional plane. *A* is the area over which the velocity distribution is integrated, and corresponds to the area of the target phase. The present ultrasound monitoring obtains the velocity distribution $u_x(y,z)$, the air–oil interfacial position $y_{ao}(z)$, and the oil–water interfacial position $y_{ow}(z)$ on the central line at $0 < y < D$, $z = 0$. Conditions for perfect stratification of the three phases implies $u_x(y,z) = u_x(y,0)$, $y_{ao}(z) = y_{ao}(0)$, and $y_{ow}(z) = y_{ow}(0)$. This simplification leads to two formulae that give simultaneously the volume flow rates of both oil and water:

$$\begin{cases} Q_o(t) = \int_{y_{ow}(0)}^{y_{ao}(0)} u_x(y, 0) \cdot 2\sqrt{y(D-y)} \cdot dy, \\ Q_w(t) = \int_0^{y_{ow}(0)} u_x(y, 0) \cdot 2\sqrt{y(D-y)} \cdot dy. \end{cases} \tag{8}$$

These quantities are computed using discrete numerical integration based on the rectangular rule, and depend on the spatial sampling interval. Note that these two independent flow rates are obtained as a function of time at a given arbitrary sampling frequency of the ultrasound measurement.

Fig. 15 shows the plots of the time-dependent flow rates for oil and water in the half-period of the pipe oscillation at sampling rate of 67 Hz. The oil phase moves earlier than the water phase and its flow rate peaks first. This is due to gravity waves in the oil phase propagating above the water phase. The water phase then flows and accelerates whereas the oil flow settles. When the water flow rate peaks, the oil flow moves again which persists after the water flow stops. Large scattering of the data in the oil flow rate near the tail of the distribution is attributed to a vertical fluctuation of the oil–water interface owing to shear-induced waves amplified. The total flow rate of oil and water phases (marked in black) increases
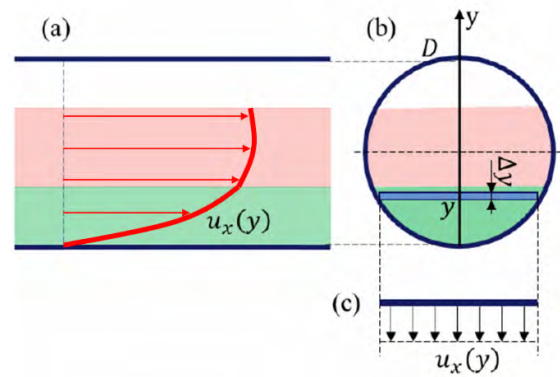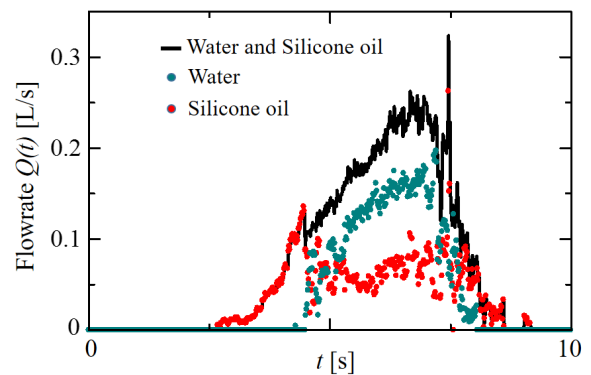
monotonically, peaks, and gradually decreases, being simpler than the behavior of the constituent flow rates. This implies that the total flow rate behaves as a two-phase flow of gas and liquid [25]–[27]; its decomposition into three phases shows no functional similarity to the total liquid flow rate. A large peak in the total flow rate in the tail comes from a three-phase flow instability, which takes place at the moment when the flow rate of water decelerates quickly and falls below that of oil. Note that, in the present experimentation platform, the volume flow rate of air is given simply by $Q_a = -(Q_o + Q_w)$ as the three phases are packed inside a single pipe with closed ends. In a long pipe without ends, the flow rate of the gas phase can be estimated using the equation of continuity for incompressible multiphase flow.

A quantitative assessment of the accuracy in flow rate measurements is possible as a cumulative flow volume is evaluated from the time-dependent constituent flow rates. The results for the cumulative flow volume for each phase (Fig. 16) were calculated using

$$V(t) = \int_{t=0}^{t} Q(t) dt. \tag{9}$$

In tests, we poured 400 mL of water and 300 mL of Silicone oil into the pipe. For the measurement system to demonstrate perfect accuracy, the cumulative flow volumes need
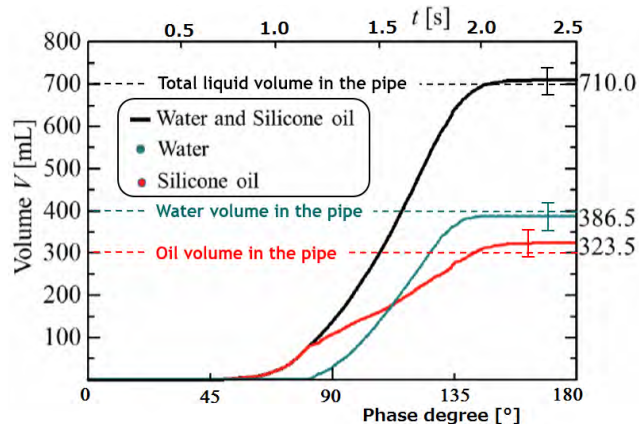
FIGURE 16. Measured cumulative flow volumes given by space-time integral of UVP-velocity data as 300 mL and 400 mL of oil and water were filled inside the pipe. Error bars indicate 10 % in relative error.

to recover these same values. The measured results in the figure indicate that the error is 3% for water and 8% for oil. The error for the total liquid flow rate is 2%. By the same assessment for the other three-phase flow conditions, the maximum error has been found to be less than 10% for constituent flow rates and 5% for total flow rates. These evaluations are notable in the single slugging motion of the three-phase flow, and in principle, therefore, the flow rate over long-duration time averages, including unsteady flow, would yield better accuracy using the sampling law, i.e. the inverse square-root principle. For instance, 10% of the random error for a single event is comparable with 5% for four events, and 1% for 100 events. In applications, we assume users will choose time-average durations depending on their needs when applying the present measurement technique.

IV. SUMMARY

An experimental technique for ultrasound monitoring of three-phase pipe flow was presented. We designed a see-saw type of pipe oscillation facility and an experimentation platform to control the internal three-phase behavior with arbitrary unsteadiness. For an in-depth analysis, multiple measurement instrumentations were mounted on the same frame. Our main focus on three-phase flow was periodic co-flowing stratified flow that accompanied multiple flow elements to evaluate the performance of ultrasound sensing. The flow features slugging wave fronts on the air–oil interface, shear-induced displacements on the oil–water interface, and turbulence in the tail of the stratified flow.

The following conclusions are drawn: (i) Ultrasound echoes are detectable from both the air–oil interface and the oil–water interface as long as the transmission occurs in the first of either liquid in the pipe; (ii) The flow velocity obtained from pulse Doppler signals is influenced by acoustic refraction at the oil–water interface leaving a bias error dependence in the flow behavior; (iii) The identification of the fluid phase is realized by thresholding the echo intensity

profile. With the identification, the virtual Doppler velocity distribution inherent in the air phase can be eliminated; and (iv) Constituent flow rates are obtained by spatial integration of velocity distribution within each identified phase. The volume error is less than 10% for a single slugging event, which is equivalent to 1% in calculations of a 100-ensemble-averaged flow rate. The next step of development is to use multiple ultrasound measurement lines, which may improve the three-dimensional monitoring of three-phase flows.

REFERENCES

[1] Y. Inoue, H. Kikura, H. Murakawa, M. Aritomi, and M. Mori, "A study of ultrasonic propagation for ultrasonic flow rate measurement," *Flow Meas. Instrum.*, vol. 19, nos. 3–4, pp. 223–232, Jun./Aug. 2008.

[2] Y. Takeda, "Velocity profile measurement by ultrasound Doppler shift method," *Int. J. Heat Fluid Flow*, vol. 7, no. 4, pp. 313–318, 1986.

[3] B. Beulen, A. C. Verkaik, N. Bijnens, M. Rutten, and F. van de Vosse, "Perpendicular ultrasound velocity measurement by 2D cross correlation of RF data—Part B: Volume flow estimation in curved vessels," *Experim. Fluids*, vol. 49, no. 6, pp. 1219–1229, 2010.

[4] M. J. W. Povey, *Ultrasonic Techniques for Fluids Characterization*. London, U.K.: Academic, 1997, pp. 11–44.

[5] B. Ourlev and E. Windhab, "Novel ultrasound based time averaged flow mapping method for die entry visualization in flow of highly concentrated shear-thinning and shear-thickening suspensions," *Meas. Sci. Technol.*, vol. 14, no. 1, pp. 140–147, 2003.

[6] T. Nakashima, T. Shiratori, Y. Murai, Y. Tasaka, Y. Takeda, and E. J. Windhab, "Viscoelastic responses of flow driven by a permeable disk investigated by ultrasound velocity profiling," *Flow Meas. Instrum.*, vol. 48, pp. 97–103, Apr. 2016.

[7] T. Wang, J. Wang, F. Ren, and Y. Jin, "Application of Doppler ultrasound velocimetry in multiphase flow," *Chem. Eng. J.*, vol. 92, nos. 1–3, pp. 111–122, 2003.

[8] H. Murakawa, H. Kikura, and M. Aritomi, "Application of ultrasonic Doppler method for bubbly flow measurement using two ultrasonic frequencies," *Experim. Thermal Fluid Sci.*, vol. 29, no. 7, pp. 843–850, 2005.

[9] Y. Murai, H. Fujii, Y. Tasaka, and Y. Takeda, "Turbulent bubbly chan-nel flow investigated by ultrasound velocity profiler," *J. Fluid Sci. Technol.*, vol. 1, no. 1, pp. 12–23, 2006.

[10] M. R. Widyanto, M. B. Utomo, K. Kawamoto, B. Kusumoputro, and K. Hirota, "Local gas holdup measurement of a bubble column using SONIA-ultrasonic non-invasive method," *Sens. Actuators A, Phys.*, vol. 126, no. 2, pp. 447–454, 2006.

[11] Y. Murai, S. Ohta, A. Shigetomi, Y. Tasaka, and Y. Takeda, "Development of an ultrasonic void fraction profiler," *Meas. Sci. Technol.*, vol. 20, no. 11, p. 114003, 2009.

[12] S. R. G. A, Y. Murai, and Y. Takeda, "Chapter 1 ultrasound-based gas–liquid interface detection in gas–liquid two-phase flows," *Adv. Chem. Eng.*, vol. 37, pp. 1–27, Dec. 2009.

[13] S. M. van der Meer *et al.*, "Microbubble spectroscopy of ultrasound contrast agents," *J. Acoust. Soc. Amer.*, vol. 212, no. 1, pp. 648–656, 2007.

[14] H. Murakawa, H. Kikura, and M. Aritomi, "Application of ultrasonic multi-wave method for two-phase bubbly and slug flows," *Flow Meas. Instrum.*, vol. 19, nos. 3–4, pp. 205–213, 2008.

[15] Y. Murai, Y. Tasaka, Y. Nambu, and Y. Takeda, S. R. G. A, "Ultrasonic detection of moving interfaces in gas–liquid two-phase flow," *Flow Meas. Instrum.*, vol. 21, no. 3, pp. 356–366, 2010.

[16] Y. Takeda, Y. Murai, and Y. Tasaka, "Ultrasonic multiphase flowmeter, ultrasonic multiphase flow rate measurement program, and multiphase flow rate measurement method using ultrasonic wave," U.S. Patent 8 401 805 B2, Mar. 13, 2013.

[17] Y. Tasaka, T. Kimura, and Y. Murai, "Estimating the effective viscosity of bubble suspensions in oscillatory shear flows by means of ultrasonic spinning rheometry," *Experim. Fluids*, vol. 56, p. 1867, Jan. 2015.

[18] H. J. Park, Y. Tasaka, and Y. Murai, "Ultrasonic pulse echography for bubbles traveling in the proximity of a wall," *Meas. Sci. Technol.*, vol. 26, no. 12, p. 125301, 2015.

[19] M. M. F. Figueiredo, J. L. Goncalves, A. M. V. Nakashima, A. M. F. Fileti, and R. D. M. Carvalho, "The use of an ultrasonic technique and neural networks for identification of the flow pattern and measurement of the gas volume fraction in multiphase flows," *Experim. Thermal Fluid Sci.*, vol. 70, pp. 29–50, 2016.

[20] G. Oddie and J. R. A. Pearson, "Flow-rate measurement in two-phase flow," *Annu. Rev. Fluid Mech.*, vol. 36, pp. 149–172, Jan. 2004.

[21] A. J. Mwambela and G. A. Johansen, "Multiphase flow component volume fraction measurement: Experimental evaluation of entropic thresholding methods using an electrical capacitance tomography system," *Meas. Sci. Technol.*, vol. 12, no. 8, pp. 1092–1101, 2001.

[22] W. Warsito and L.-S. Fan, "Measurement of real-time flow structures in gas–liquid and gas–liquid-solid flow systems using electrical capacitance tomography (ECT)," *Chem. Eng. Sci.*, vol. 56, nos. 21–22, pp. 6455–6462, 2001.

[23] Y. Murai, Y. Matsumoto, and F. Yamamoto, "Three-dimensional measurement of void fraction in a bubble plume using statistic stereoscopic image processing," *Exp. Fluids*, vol. 30, no. 1, pp. 11–21, 2001.

[24] E. Hervieu, E. Jouet, and L. Desbat, "Development and validation of an X-ray tomography for two-phase flow," *Ann. New York Acad. Sci.*, vol. 972, no. 1, pp. 87–94, 2002.

[25] Y. Murai, H. Oiwa, T. Sasaki, K. Kondou, S. Yoshikawa, and F. Yama-moto, "Backlight imaging tomography for gas–liquid two-phase flow in a helically coiled tube," *Meas. Sci. Tech.*, vol. 16, no. 7, pp. 1459–1468, 2005.

[26] Y. Murai, S. Yoshikawa, S. Toda, M. Ishikawa, and F. Yamamoto, "Structure of air–water two-phase flow in helically coiled tubes," *Nucl. Eng. Des.*, vol. 236, no. 1, pp. 94–106, 2006.

[27] Y. Murai, K. Inaba, Y. Takeda, and F. Yamamoto, "Backlight imaging tomography for slug flows in straight and helical tubes," *Flow Meas. Instrum.*, vol. 18, nos. 5–6, pp. 223–229, 2007.

YUICHI MURAI received the Ph.D. degree in engineering from the University of Tokyo in 1996. He was involved in nuclear engineering with Fukui University and applied optics with the Imperial College London from 1995 to 2012. He has been a Full Professor with Hokkaido University since 2010. His research interests are dynamics of multiphase flows, measurement techniques of fluid flows, and renewable energy.

HYUN JIN PARK received the Ph.D. degree from Hokkaido University in 2016. He was with LG Electronics Inc. and the Institut de Mécanique des Fluides de Toulouse. He has been an Assistant Professor with Hokkaido University since 2016. His research interests are ship drag reduction, multiphase flow, ultrasound technology, PIV, image processing, laser applications, and signal processing for various thermo-fluid physics and engineering systems.

JUNPEI HITOMI received the degree from the Department of Mechanical Intelligence System Engineering, Hokkaido University, in 2017. He received the Hatakeyama Prize given for best students in the field of mechanical engineering and from the Japan Society of Mechanical Engineers in 2017. His main research is the development of ultrasound techniques for dynamic multiphase flow systems.

YUJI TASAKA received the Ph.D. degree from Hokkaido University in 2004. He started his professional research career with Hokkaido University, as a Research Associate, and where he has been an Associate Professor since 2011. His research interests are flow instability and transition phenomena, as well as the development of measurement techniques.

• • •